

International Conference on Space Optics—ICSO 2006

Noordwijk, Netherlands

27–30 June 2006

Edited by Errico Armandillo, Josiane Costeraste, and Nikos Karafolas



Progress in static fourier transform infrared spectroscopy: assessment of sifti preliminary performances

*Philippe Hébert, Clémence Pierangelo, Alain Rosak,
Elodie Cansot, et al.*



PROGRESS IN STATIC FOURIER TRANSFORM INFRARED SPECTROSCOPY: ASSESSMENT OF SIFTI PRELIMINARY PERFORMANCES

Philippe Hébert⁽¹⁾, Clémence Pierangelo⁽¹⁾, Alain Rosak⁽¹⁾, Elodie Cansot⁽¹⁾, Frédéric Bernard⁽¹⁾,
Claude Camy-Peyret⁽²⁾

⁽¹⁾ CNES, CST, 18 av. E. Belin, 31401 Toulouse Cédex 9 – France

⁽²⁾ LPMAA, UMR7092, Université Pierre et Marie Curie / CNRS, Case 76, 4 Place Jussieu, F-75252 Paris CEDEX 05,
France

ABSTRACT

The concept of static Fourier transform interferometry at thermal infrared wavelengths is well suited in the case of narrow spectral bands that are looked at for targeted molecular species as CO and O₃ for pollution and air quality monitoring, or H₂O and CO₂ for weather forecast, down to the troposphere. It permits a high spectral resolution and a very good radiometric performance, with the advantage of a static interferometer, including no moving part. Along with other molecules sounded in the UV-VIS domain, as for instance in the TRAQ mission, SIFTI will provide scientists with a complete set for pollution measurements and air quality survey.

Our paper presents the principles of static Fourier transform spectrometry, the work led on the instrument performance model and our study of the SIFTI instrument. We describe the instrument, its main dimensions and characteristics, and its architecture and major subsystems. We eventually make a preliminary survey of the SIFTI performance budget items.

As a conclusion, we introduce the future CNES phase A study of this instrument that is started in 2006

1. Introduction

In the field of space remote sensing, one application of infrared sounding is the monitoring of the atmospheric pollution, with the goal of getting information pieces about atmospheric components down to the boundary layer.

Proposed as a response to the ESA's "Earth Explorer" call for ideas, the TRAQ mission defines a payload within a space borne system that meets this objective. Set within a Netherlands-France partnership, the mission includes 3 complementary instruments onboard a Minisat satellite on a low earth orbit:

TROPOMI (NL): a UV/Vis spectrometer, derived from OMI (NL), for NO₂, H₂CO and SO₂ sounding;

SIFTI (F): a Static Infrared Fourier Transform Interferometer, derived from the MOLI concept [1], and adapted to infrared for CO and O₃ sounding;

OCAPI: an extended version of PARASOL (F) for aerosol detection;

SIFTI includes the CLIM imager, used for cloud field characterization.

As for SIFTI, the detection of O₃ and CO needs only narrow spectral bands, which allows the use of the static Fourier transform interferometer (or "facet interferometer") that simplifies the mechanical design greatly. The sounding footprint is a single pixel type, possibly with an agile scan to deal with clouds.

2. Mission objectives and instrument requirements

The scientific objective of a space mission for the global monitoring of pollution is to reach a better understanding of the impact of anthropogenic activities and of natural phenomena on the troposphere composition, over Europe, especially through the measurements of diurnal, seasonal, annual ... variations of the implied species. As for the infrared part of the spectrum, covered by SIFTI, the first step is to demonstrate the feasibility of the CO and O₃ profile retrieval. That is to say to get 4 to 6 degrees of freedom for concentrations in the depth of the atmosphere. The first measurement point (in the low troposphere) is of most importance. The accuracy needed in the vertical profiles is of the order of 10 to 20 %.

Molecules are sounded in 2 spectral bands: B1 = [1030 – 1070 cm⁻¹] (~ 9.5 μm) for O₃ and B2 = [2100 – 2140 cm⁻¹] (~ 4.7 μm) for CO.

Spectral resolution should be at least $d\sigma_{\text{apod}}=0.125 \text{ cm}^{-1}$ after apodization.

A 2 hour revisit time will be insured by the non-synchronous drifting orbit at 716 km altitude.

The spatial sampling on ground aims to be 50 km at nadir, and the spatial resolution, i.e. the diameter of the pixel on ground, will be 10 km at nadir. The goal is to obtain at least 25 measurement points in the ±850 km with respect to nadir swath.

The CLIM imager shares a common scan mirror with the sounder.

The first instrumental option is a third spectral band B3 = [4270 – 4300 cm⁻¹] (2.3 μm) that is used to force the CO column amount by daytime, in terms of reflected / backscattered solar flux, in the profile retrieval process, and then enhance the accuracy of the later. This band can be implemented either in TROPOMI or in SIFTI. Further studies will assess the best compromise. The second option deals with an agile pointing scan. This should enhance the rate of clear pixels by a factor 2.5 [2] because this system is designed to stare the line of sight of the sounder at cloud clear zones within each 50 km × 50 km Field Of Regard, as symbolized in Figure 1:

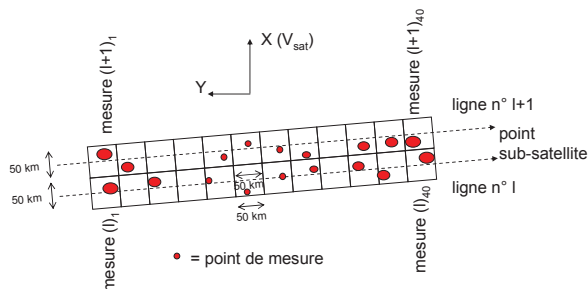


Figure 1: schematic of the agile pointing along two successive swaths

Radiometric requirements are expressed as an objective of a noise equivalent temperature discrepancy (NEDT) better than 65 mK in B1 and 73 mK in B2. The instrument shall be designed to meet this specification, and the study of the B3 band will determine its performance as is. SIFTI will be designed as for a demonstration mission, with a life time of 3 years.

3. Instrument specification rationale

Relationship between instrument performances (e.g. spectral resolution, noise...) and retrieval performance (e.g. accuracy of the gaz concentration retrieved, vertical resolution...) must be investigated using forward and inverse modelling. Forward modelling is performed with a very fast line-by-line radiative transfer code, 4AOP [3,4]. Performances of the retrieval algorithm are evaluated in the framework of optimal estimation theory [5].

3.1. Selection of spectral bands and spectral resolution

SIFTI spectral bands have been chosen according to the presence of absorption lines of targeted species, CO and O₃ (Figure 2). Band 1, for ozone retrieval, covers the spectral range 1030-1070 cm⁻¹ and Band 2, for CO retrieval, covers the spectral range 2100-2140 cm⁻¹.

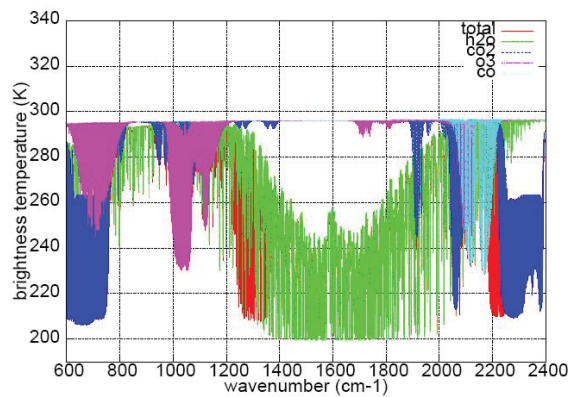


Figure 2: contribution of selected molecules in the atmospheric spectrum : H₂O (green), CO₂ (blue), O₃ (pink), CO (cyan). 4AOP simulations.

A high spectral resolution is required in order to resolve the spectral absorption lines of the targeted molecule, thus enabling vertical sounding and retrieval of the molecular profile (the higher the gas absorption, the higher the observed altitude range). However, the choice of spectral resolution results from a trade-off between the need of a high resolution and the width of the spectral band considered. Therefore, the compromise chosen is a 40 cm⁻¹ wide band with an unapodised spectral resolution of 0.0625 cm⁻¹. With such a spectral resolution, the CO lines are fully resolved but the ozone lines are not (Figure 3).

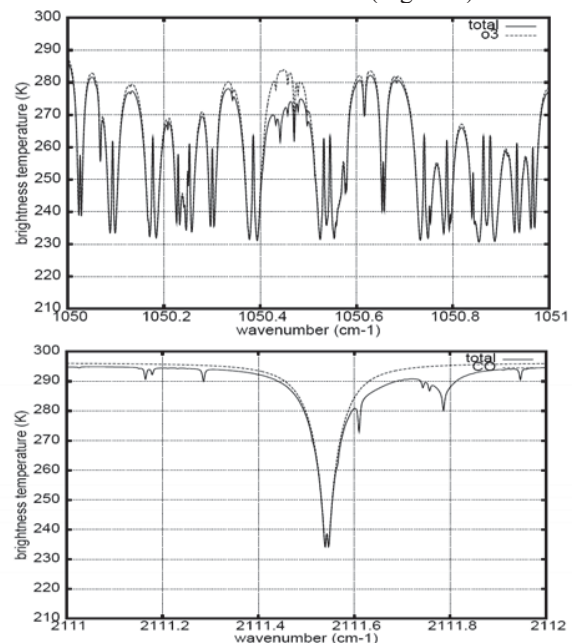


Figure 3: brightness temperature (K) as a function of wavenumber for a narrow spectral band (1 cm⁻¹): at SIFTI spectral resolution, the O₃ absorption lines are not resolved (top) but the CO absorption lines are resolved (bottom).

3.2. Impact of instrumental noise on retrieved gas concentrations

The formalism of optimal estimation provides a way to estimate the impact of different sources of error on the final error of the retrieved product. Thus, by comparing the contribution of instrumental noise with the contribution of uncertainty on model parameters (e.g. surface temperature, water vapour amount...), we get a value for the maximum instrument noise that can be accepted.

4. Extended Shannon criteria, SIFTI principle

In the case of a narrow spectral band, where the useful spectral interval is limited to $\Delta\sigma = \sigma_{\max} - \sigma_{\min}$, the spectrum can be reconstructed from an interferogram sampled at intervals of path difference of only

$$\delta'_{ech} = \frac{1}{2 \cdot (\sigma_{\max} - \sigma_{\min})} \quad (1)$$

This will be possible provided that $\sigma_{\max}/(\sigma_{\max}-\sigma_{\min})$ is an integer, and that the spectrum is zero below σ_{\min} and above σ_{\max} [6]. This latter condition must be undertaken by a narrow optical filter, in front of the detectors, to avoid spectrum aliasing, as in Figure 4:

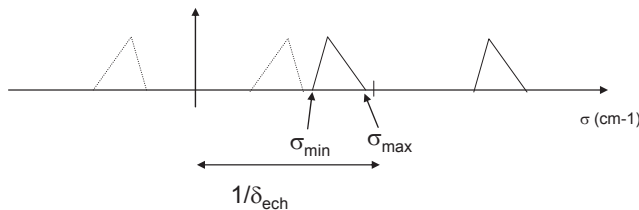


Figure 4 : Avoiding spectrum aliasing with a narrow filter

The narrow spectral bands required by the mission make it suitable to the SIFTI principle. The interferometer can be seen as the superposition of N_b Michelson interferometers with a fixed set of Optical Path Difference (OPD), as depicted in Figure 5:

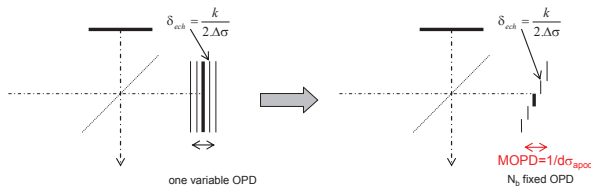


Figure 5: from the dynamic to the static Fourier transform interferometer

Of course the pupilla of each OPD is N_b times less than in a classical interferometer, but the integration time of each OPD is N_b times greater, so the later balances the former. Actually, the benefit of the principle is to save a translation mechanism, resulting in a significant opto-electro-mechanical simplification.

The interferogram being single sided in our case, the number of samples is given by:

$$N_b = \frac{2 \cdot (\sigma_{\max} - \sigma_{\min}) \cdot M_{TF}}{d\sigma_{apod}} \quad (2)$$

where M_{TF} is the margin on the spectral width of the optical filter w.r.t the useful bandwidth. We assume that the filter has a zero transmission outside a bandwidth of $(\sigma_{\max}-\sigma_{\min}) \cdot M_{TF}$, with $M_{TF} = 1.5$ for technological reasons. Numerical application yields $N_b = 960$. With a facet mirror of $32 \times 32 = 1024$ facets, we obtain a margin of 64 samples in the negative part of the interferogram, useful for Zero Path Difference (ZPD) determination. Thus the Fourier transform provides 960 useful spectral samples, spaced by $\delta_{ech} = \delta'_{ech}/M_{TF} = 83 \mu\text{m}$.

However, one has to deal with the actual, not perfect, location of the facets, thus the OPDs, before performing the Fourier transform. This process is called the "reconstruction" of the interferogram [7]. In the ideal case where the facets are perfect, the measured interferogram expresses as:

$$i_r(x) = i(x) \cdot \sum_{k=-\infty}^{+\infty} \delta(x - k \cdot \delta_{ech}) \times f(x) \quad (3)$$

where $f(x)$ is the inverse Fourier transform (FT^{-1}) of the narrow filter spectral transmittance. This can also be written as:

$$i_r(x) = \sum_{k=0}^{+\infty} i(k \cdot \delta_{ech}) \cdot [f(x - k \cdot \delta_{ech}) + f(x + k \cdot \delta_{ech})] \quad (4)$$

In the case where a location error α_k occurs for each sample, the measured interferogram becomes:

$$i_r(k' \delta_{ech} + \alpha_{k'}) = \sum_{k=0}^{+\infty} i(k \cdot \delta_{ech}) \cdot [f((k'-k) \cdot \delta_{ech} + \alpha_{k'}) + f((k'+k) \cdot \delta_{ech} + \alpha_{k'})] \quad (5)$$

Eq. 5 can be written under a matrix form: $I_\alpha = T \cdot I$. One has to inverse it: $I = T^{-1} \cdot I_\alpha$ to reconstruct the actual interferogram from the measured one. The error α_k has to be known with an accuracy, classical in infrared interferometer, of several nanometres. Tolerance of the reconstruction processing to radiometric noise and OPD jitter has been subject to CNES studies [8]. The static spectrometry principle and the associated algorithms are under a CNES patent.

The facets of the interferometer are imaged onto two 2D detector, cooled to a suitable temperature to infrared wavelengths. The spectral bands are previously separated by dichroics.

5. Instrument radiometric items

The transfer of the noise from interferogram to spectrum leads to challenging figures for the Signal to

Noise Ration (SNR) to be reached in interferograms, at the output of the detectors.

5.1. Signal

The number of signal electrons is determined by:

- the integration time of 110 ms, taking into account the orbit, the swath, the number of measurements in the footprint, the cinematic of the scan mechanism, and the calibration strategy;
- the spectral sampling of $\delta\sigma = 0.0625 \text{ cm}^{-1}$;
- the étendue defined by the pixel, the altitude and the aperture of the instrument (a $100 \text{ mm} \times 100 \text{ mm}$ square);
- the transmission of the instrument, and the contrast of the interferometer, leading to an efficiency of 0.32;
- the quantum efficiency of the detectors, assumed to be 0.55 and 0.7 in B1 and B2 respectively;
- the radiance of the target. It is modelled as a black body emission at a temperature between 270 K and 290 K, multiplied by a pseudo atmospheric transmission that is normalized. Indeed the relative shape of the spectra (and not its absolute level given by the temperature) in the O_3 and the CO spectral ranges is quite a constant w.r.t atmospheric conditions. This is summarized in Figure 6:

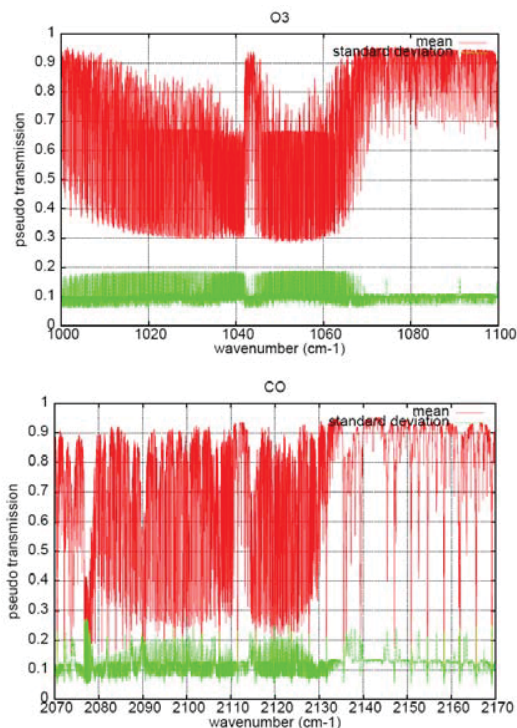


Figure 6: Average (red) and standard deviation (green) of atmospheric transmission for O_3 (above) and CO (below) region, among 232 atmosphere cases.

The radiometric performances are required for a black body source at 280K seen through this average transmission. For warmer black bodies the radiometric performances will be better. A majority of the atmospheric cases encountered over mid-latitude countries correspond to an equivalent black body temperature greater or equal to 280 K.

5.2. Noises

Different noise sources are to be considered:

- the photon noise from the signal itself;
- the photon noise from the instrument background. We assume a global emissivity of 0.135, and an instrument temperature of 273 K;
- the variation (between calibrations) of the gradient of this parasitic emission;
- the photon noise and the flux gradient variation of the cooled detector box;
- the noise of the dark current, assuming detectors at 65 K and 90 K for B1 and B2 respectively;
- the fluctuations of the gradient of the dark current within the detectors;
- the read out noise;
- the 1/f noise;
- the electronic chain noises, including quantization;

Furthermore, one has to add the noise induced by the OPD sampling error, and the noise caused by diffraction. Indeed, the imagery of facets onto the detectors is made through a field stop, who's aperture brings smearing between facet images due to diffraction.

Besides, the Pixel Response Non Uniformity (PRNU) must be accounted for.

6. Synoptic of the instrument

6.1. Data processing

In order to lower the effects of different noises and fluctuations, several processing of the acquisitions are implemented.

The radiometric calibration is the most classical one. It aims at calibrate the spectra in terms of radiance temperatures. For that, SIFTI looks periodically at an internal black body and at deep space. Then we apply eq. 6 to every atmospheric spectra $N(\sigma)$ to get the actual emitted radiance $B(\sigma)$:

$$B(\sigma) = B_{BB}(\sigma, T_{BB}) \cdot \text{Re} \left(\frac{N(\sigma) - N_{CS}(\sigma)}{N_{BB}(\sigma) - N_{CS}(\sigma)} \right) \quad (6)$$

where N is a measured spectrum, B_{BB} is the Planck function for the black body (which temperature T_{BB} must be accurately monitored), "BB" stands for black body and "CS" for cold space. This calibration occurs after Fourier transforms. Both can be made on ground,

because the limited number of interferogram samples allows to download interferograms.

The need for reconstruction was presented in § 4. It implies to get the actual position of each OPD. This can be made by a reference sub-system based on a very stable laser which provides, parallel to the interferograms and possibly at the same time, a set of relative positions of each facet. This data set is injected in eq. 5.

Phase modulation is an innovative way to reduce the effect of inter-pixel offsets, stray light fluctuations and to reduce noise effects. Let us call λ_{av} the medium wavelength of the spectral band. Four interferograms are acquired during the integration time, separated by an OPD of $\lambda_{av}/8$: I_1, I_2, I_3 and I_4 . The differences I_2-I_1 and I_4-I_3 give the derivatives of the interferogram, thus reduce the effect of background and offset slow variations. Processing I_2-I_1 and I_4-I_3 allows to double the number of samples, then to increase the stability and the performance of the reconstruction algorithm with respect to noise.

6.2. Hardware

Figure 7 presents the main instrument subsystems:

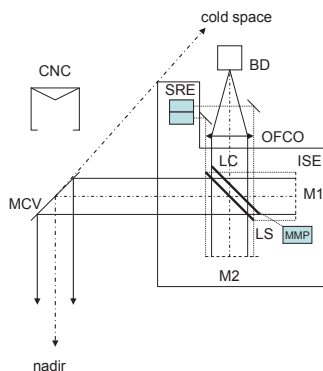


Figure 7 : Functional layout of SIFTI

- MCV = Scanning mirror: insures the cover of the swath and the view on calibration targets;
- CNC = Calibration black body: provides the knowledge of $B_{BB}(\sigma, T_{BB})$ in eq. 6;
- M_i = (facet) mirrors ($\times 2$): form the 32×32 OPDs;
- LS = Beam splitter: separates the incident beam into 2 equal parts and recombines them;
- LC = compensating plate: equalizes the depth of glass crossed by light in the two harms of the interferometer. It may be translated closed to M1;
- SRE = sampling reference subsystem: based on a very stable laser, provides the accurate knowledge of each OPD for each interferogram;
- MMP = phase modulation subsystem: allows to get 4 interferograms separated by $\lambda_{av}/8$. May be

based on piezo actuators. May act on the compensator or on one mirror;

- ISE = interferometer;
- OFCO = focusing optics: focuses the image of the earth onto the entrance of the detector box;
- BD = detector box: transfers the optical signal into an electrical current; defines a cold pupilla; images the facets onto the detectors; defines the field of view; separates the two (or three) spectral bands; passively cools down the optics, and actively the detectors. The architecture of the BD is of the same kind as for IASI, as depicted in Figure 8:

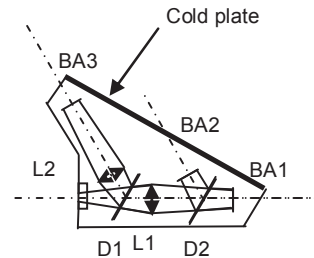


Figure 8 : Functional layout of the detector box

The narrow optical filters have a width of 363 nm, 89 nm and 16 nm in B1, B2 and B3 respectively. A previous R&T study validated the feasibility of 6 nm large filters in the near infrared, and a future study is foreseen in 2006 for the extension to thermal infrared.

Facet mirrors were subjects to R&T studies and to prototypes development shown in Figure 9:

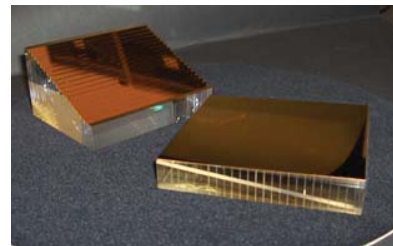


Figure 9: facet mirror prototypes (CNES R&T)

Including these subsystems, the opto-mechanical concept leads to Figure 10:

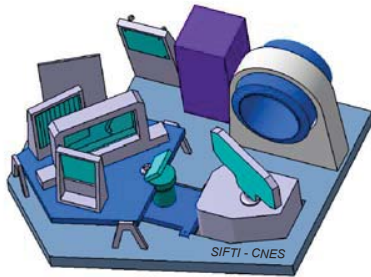


Figure 10: SIFTI opto-mechanical layout

7. Preliminary budgets

The instrument lies within a box of 1 m × 0.6 m × 0.3 m, the cryogenic machines being deported in the platform. To date, the mass is evaluated to 70 kg, and the power between 100 and 150 W, mainly due to the cryogenic machines.

The relative weigh of each noise item is given by Figure 11:

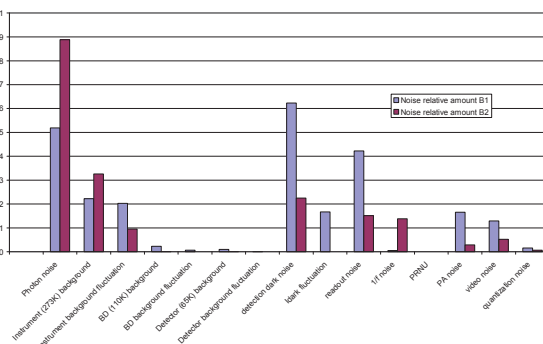


Figure 11: relative weigh of noise items

One can see that B1 is limited the dark current of the detector, and that B2 is limited by the photon noise. This implies that the future phase A study shall focus particularly on the cooling of the detector, possibly down to 60 K for B1 detector, and on the compromise between the size of the instrument aperture and the number of scanning positions along a line, in order to improve the radiometric performance. To date, the SNR of the interferogram is estimated to be 15000 for B1 and 5000 for B2.

8. Conclusion

We have presented the mission of SIFTI, its instrumental principle and concept, resulting from our phase 0 studies. SIFTI's concept is well suited for this narrow spectral band sounding mission, but the required performances showed to be very challenging. Our future works will include a phase to consolidate

the expression of the requirements for the system and the instrument, and a more classical one for instrument feasibility and definition study during a phase A to start end 2006. This shall allow to consolidate the results presented here above, as to prepare, if successful, the development phases in the best conditions, for a launch due date in 2013.

9. References

1. P. Vermande et al, Spectroscopie par transformée de Fourier des spectres étroits. Application aux interféromètres statiques, in ICSO 2000 Proceedings.
2. T. Phulpin, C. Camy-Peyret et al, TRAQ, une mission pour le suivi global de la pollution atmosphérique, in AEI 2006.
3. Scott, N.A. and A. Chedin, 1981: A fast line-by-line method for atmospheric absorption computations: The Automatized Atmospheric Absorption Atlas. J. Appl. Meteor., 20, 556-564.
4. L. Chaumat, N. Decoster, C. Standfuss, B. Tournier, R. Armante and N.A. Scott, 2003: 4A/OP Reference Documentation, NOV-3049-NT-1178-v2.2, NOVELTIS, LMD/CNRS, CNES, 232 pp.
5. Rodgers, C.D., Inverse methods for atmospheric sounding, Theory and Practice, Series on Atmospheric, Oceanic and Planetary Physics-Vol. 2, World Scientific, 2000.
6. R. Beer, Remote Sensing by Fourier Transform Spectrometry, Chemical Analysis vol. 120, Wiley-Interscience publication, 1992
7. A. Rosak and F. Tinto, Progress Report of a static Fourier Transform spectrometer Breadboard, in ICSO 2004 Proceedings
8. A. Rosak and F. Tinto, Static Fourier Transform Spectrometer for CO₂ monitoring, in Horizons de l'optique 2003